Photogenerated Charge Storage in Hetero-Langmuir–Blodgett Films

Katsuyuki Naito* and Akira Miura

Contribution from the Advanced Research Laboratory, Research and Development Center, Toshiba Corporation, 1 Komukai-Toshiba-cho, Saiwai-ku, Kawasaki 210, Japan

Received October 19, 1992

Abstract: Photoinduced electron transfer (charge separation) and back electron transfer (charge recombination) were investigated for the following hetero-Langmuir–Blodgett film device: ITO//insulator layers, 185 Å/two layers of steroidal tetracyano-*p*-quinodimethane as an acceptor (A), 36 Å/two layers of a Cu-phthalocyanine derivative as a sensitizer (S), 28 Å/two layers of steroidal *p*-phenylenediamine as a donor (D), 48 Å/insulator layers, 380 Å//Hg or Al. A transient electric current was observed by the selective photoexcitation of S and was ascribed to the net electron transfer from D to A. The resulting charge separation state in the ASD device survived for a few minutes. Applying electric biases and/or lowering temperatures caused the charge-separated state to last much longer. The charge recombination process observed for the ASD structure could not be described by the usual first-order reaction kinetics. We have elucidated the charge recombination mechanism on the basis of the Marcus theory by taking account of some distribution effects of both the activation energies and distances between the dye layers. The results of the lowering of the temperature (290 → 110 K) indicated a wide distribution of the activation energy (D_E), suggesting a distribution of free energy change during the electron transfer. The free energy change distribution (D_G) was found to be nearly in accordance with the product of the Gaussian distribution of the energy levels for charge-separated states and the Fermi distribution of the electric charges. Insertion of insulator layers between A and S also brought a distance distribution between A and S, which was probably caused by some structural defects in the insulator layers. The charge separation processes are also discussed.

Introduction

Molecular electronic devices (MEDs) have been attracting much attention in expectation that they are superior to present inorganic solid devices.[1] Carter proposed an idea for various MEDs consisting of conjugated polymer chains, along which the motions of charged carriers or of solitons were controlled by an external electric field.[2] Aviram et al. proposed molecular rectifiers using the intramolecular electron transfer between donor and acceptor moieties,[3] and many attempts to realize them have been done since then.[4] Wilson et al.[5] and Hopfield et al.[6] intended to fabricate molecular charge-shift registers having an almost similar function to the present charge-coupled devices. The former group observed a rapid electron transfer between the dye layers in homo-Langmuir–Blodgett films, caused by both an electric field and a light pulse.[7] These ideas seem to be aimed at molecular-based information processors, where various elementary processes such as charge injection from electrodes or carrier photogeneration in organic superlattices under an applied electric field may play fundamental roles. Many memory or switching phenomena in organic solid films have been examined as prototypical candidates for MEDs.[8] However, their mechanisms have not been well elucidated, and their interpretations have sometimes been controversial. The proposed device characteristics have not yet been rationalized, and much effort to confirm the ideas are still incomplete. One of the main causes is thought to be that the device structures have not usually been constructed as designed because of the difficulties in controlling the molecular-level structures and in synthesizing the molecules to be used.

As for well-designed molecular systems, photosynthetic reaction centers, where several donor and acceptor moieties are oriented precisely in an ordered arrangement,[9] have been regarded as archetypes of real molecular devices.[10] The mechanism of photoinduced electron transfer (PET) has been vigorously investigated from theoretical[11] and experimental[12] standpoints

(1) For example: (a) Ashwell, G. J., Ed. *Molecular Electronics: Research Studies*; John Wiley & Sons: New York, 1992. (b) Rambidi, N. G.; Chernavskii, D. S.; Sandlewr, Yu. M. *J. Mol. Electron.* **1991**, *5*, 105. (c) Swalen, J. D.; Allara, D. L.; Andrade, J. D.; Chandross, E. A.; Garoff, S.; Israelachvili, J.; McCarthy, T. J.; Murray, R.; Pease, R. F.; Rabolt, J. F.; Wynne, K. J.; Yu, H. *Langmuir* **1987**, *3*, 932. (d) Girling, I. R.; Kolinsky, P. V.; Cade, N. A.; Earls, J. D.; Peterson, I. R. *Optics Commun.* **1985**, *55*, 289. (e) Blinov, L. M.; Dubinin, N. V.; Mikhnev, L. V.; Yudin, S. G. *Thin Solid Films* **1984**, *120*, 161. (f) Roberts, G. G. *Contemp. Phys.* **1984**, *25*, 109. (g) Carter, F. L., Ed. *Molecular Electronic Devices*: Dekker: New York, 1983.

(2) Carter, F. L. *NRL Memo. Rep.* **1979**, *3960*, 121.

(3) (a) Farazdel, A.; Dupuis, M.; Clementi, E.; Aviram, A. *J. Am. Chem. Soc.* **1990**, *112*, 4206. (b) Aviram, A. *J. Am. Chem. Soc.* **1988**, *110*, 5687.

(4) (a) Martin, A. S.; Sambles, J. R.; Ashwell, G. J. *Phys. Rev. Lett.* **1993**, *70*, 218. (b) Aviram, A. *J. Mol. Electron.* **1988**, *4*, S99. (c) Metzger, R. M.; Schumaker, R. R.; Cava, M. P.; Laidlaw, R. K.; Panetta, C. A.; Torres, E. *Langmuir* **1988**, *4*, 298.

(5) Ahmed, F. A.; Wilson, E. G. *Synth. Met.* **1988**, *27*, B593.

(6) Hopfield, J. J.; Onuchic, J. N.; Beratan, D. N. *J. Phys. Chem.* **1989**, *93*, 6350.

(7) (a) Donovan, K. J.; Sudiwala, R. V.; Wilson, E. G. *Mol. Cryst. Liq. Cryst.* **1991**, *194*, 337. (b) Donovan, K. J.; Paradiso, R.; Scott, K.; Sudiwala, R. V.; Wilson, E. G.; Bonnett, R.; Wilkins, R. F.; Batzel, D. A.; Clark, T. R.; Kenney, M. E. *Thin Solid Films* **1992**, *210/211*, 253.

(8) For example: (a) Sakai, K.; Kawada, H.; Takamatsu, O.; Matsuda, H.; Eguchi, K.; Nakagiri, T. *Thin Solid Films* **1989**, *179*, 137. (b) Tachibana, H.; Nakamura, T.; Matsumoto, M.; Komizu, H.; Manda, E.; Niino, H.; Yabe, A.; Kawabata, Y. *J. Am. Chem. Soc.* **1989**, *111*, 3080. (c) Machida, Y.; Saito, Y.; Taomoto, A.; Nichogi, N.; Waragai, K.; Asakawa, S. *Jpn. J. Appl. Phys.* **1989**, *28*, 297. (d) Villeret, B.; Nechtschein, M. *Phys. Rev. Lett.* **1989**, *63*, 1285. (e) Ottenbacher, D.; Schierbaum, K. D.; Göpel, W. *J. Mol. Electron.* **1991**, *7*, 79. (f) Nishino, Y.; Inoue, E. *Photogr. Sci. Eng.* **1981**, *25*, 35. (g) Nakazawa, Y.; Hoshino, K.; Hanna, J.; Kokado, H. *Jpn. J. Appl. Phys.* **1989**, *28*, 2517.

(9) Deisenhofer, J.; Epp, O.; Miki, K.; Huber, R.; Michel, H. *J. Mol. Biol.* **1984**, *180*, 385.

(10) Haarer, D. *Angew. Chem., Int. Ed. Engl. Adv. Mater.* **1989**, *28*, 1544.

(11) For example: (a) Moser, C. C.; Keske, J. M.; Warncke, K.; Farid, R. S.; Dutton, P. L. *Nature* **1992**, *335*, 796. (b) Marcus, R. A.; Sutin, N. *Biochim. Biophys. Acta* **1985**, *811*, 265. (c) Kakitani, T.; Mataga, N. *J. Phys. Chem.* **1988**, *92*, 5059. (d) Ulstrup, J.; Jortner, J. *J. Chem. Phys.* **1975**, *63*, 4358. (e) Hopfield, J. J. *Proc. Natl. Acad. Sci. U.S.A.* **1974**, *71*, 3640.

(12) For example: (a) Bixon, M.; Jortner, J. *J. Phys. Chem.* **1986**, *90*, 3795. (b) McDowell, L. M.; Kirmaier, C.; Holten, D. *J. Phys. Chem.* **1991**, *95*, 3379. (c) Warden, J. T., Jr.; Mohanty, P.; Bolton, J. R. *Biochem. Biophys. Res. Commun.* **1974**, *59*, 872. (d) Gunner, M. R.; Dutton, P. L. *J. Am. Chem. Soc.* **1989**, *111*, 3400. (e) Furuno, T.; Takimoto, K.; Kouyama, T.; Ikegami, A.; Sasabe, H. *Thin Solid Films* **1988**, *160*, 145.

0002-7863/93/1515-5185$04.00/0

by many researchers. With the aid of these results, many artificial systems applying PET have been investigated to elucidate such molecular devices.[13] Many molecules with chromophore moieties have been synthesized for investigating the relation between chromophore arrangement and PET kinetics mainly in a homogeneous phase, i.e., in a solution,[14] in a frozen medium,[15] and in a polymer matrix.[16] In a heterogeneous phase, i.e., in a micelle,[17] in a black membrane,[18] and in an evaporated film,[19] vectorial PETs have been designed to use photoenergy efficiently. The reaction kinetics in heterogeneous phases, however, is generally too complicated to be analyzed quantitatively. Controlling the PETs with an electric field[20] and with a magnetic field[21] has also been attempted.

As for fabricating MEDs, the Langmuir–Blodgett (LB) method[22] has been expected to be one of the most useful techniques for constructing organic thin films with highly-ordered molecular arrays or superlattices with different kinds of molecules. Pioneering studies have been carried out on PETs in LB films by Kuhn,[23] Möbius,[24] Sugi,[25] Bolton,[26] and their collaborators. More recently, Fujihira et al.[27] synthesized new amphiphilic molecules containing plural dye moieties in one molecule and reported PET in monomolecular LB films. Many other studies on PETs in LB films have been carried out.[28] The characteristics of photoelectric energy conversion have been examined, although the detailed molecular arrangements and film structures have not been well clarified.

We believe that controlling the characteristics of electric carrier flows and storage within a well-defined molecular assembly is a key technology for operating MEDs. Uniform monomolecular films with structural perfection are strongly required for the purpose. However, the presence of structural inhomogeneities and microdefects in conventionally built LB films, particularly observed in films containing functional dyes, has prevented studying their optical and electrical characteristics in a high electric field and elucidating physicochemical events. The situation is considered mainly to be rooted in the uncriticized and simple idea for designing LB molecules: introducing long alkyl chains and/or hydrophilic heads into parent dye skeletons.

Consequently, most of the efforts devoted to performing photogenerated charge control with an electric field have still been incomplete, although charge control in a well-designed organic superlattice is of vital importance to make a step forward for MEDs.

We have previously synthesized several strong donor and acceptor amphiphiles substituted by a steroid skeleton and have demonstrated that these molecules are capable of producing uniform dye LB films.[29-32] We have also investigated polymer amphiphiles of insulators[33] and a large dye amphiphile containing phthalocyanine,[34] which afforded homogeneous LB films. In the present study, we have constructed an organic superlattice device including strong donor and acceptor LB molecules: ITO transparent electrode//insulator/acceptor (A)/photosensitizer (S)/donor (D)/insulator//metal electrode. In a previous letter,[35] we have reported some preliminary results regarding PET from D to A embedded in a hetero-LB film and the field dependence of charge-storage properties. This paper reports further advanced experimental results on PET and on separated charge recombination (CR). Their mechanisms are also discussed on the basis of electron-transfer theories and structural characteristics of the hetero-LB film.

Experimental Section

Materials and Film Formation. Steroidal tetracyano-*p*-quinodimethane (TCNQ, A)[31] and steroidal *p*-phenylenediamine (D)[32] were synthesized. A Cu-phthalocyanine derivative substituted by oligomer chains of methacrylate esters (S)[34] was supplied from Dainichi Seika (Japan). Poly(isobutyl methacrylate) (PIBM) (Du Pont, Elvacite 2045)[33] and stearic acid (Wako, Japan) were used for the insulator LB films. Y-type hetero-LB films were constructed on ITO-sputtered glass plates (50 × 25 × 0.5 mm^3) by the usual vertical dipping method. The deposition conditions were as follows: subphase, freshly deionized and filtered water, 18 °C, no additives except a 0.5 mmol/L $CdCl_2$ solution only for stearic acid; dipping speed, 5 mm/min for A, D, PIBM, and stearic acid and 1

(13) For example: Fox, M. A., Chanon, M., Eds. *Photoinduced Electron Transfer*: Elsevier: Amsterdam, 1988; Vols. A–D.

(14) For example: (a) Gust, D.; Moore, T. A. *Science* **1989**, *244*, 35. (b) Gust, D.; Moore, T. A.; Makings, L. R.; Liddell, P. A.; Nemeth, G. A.; Moore, A. L. *J. Am. Chem. Soc.* **1986**, *108*, 8028. (c) Gould, I. R.; Ege, D.; Moser, J. E.; Farid, S. *J. Am. Chem. Soc.* **1990**, *112*, 4290. (d) Liang, N.; Miller, J. R.; Closs, G. L. *J. Am. Chem. Soc.* **1990**, *112*, 5353. (e) Meade, T.; Gray, H. B.; Winkler, J. R. *J. Am. Chem. Soc.* **1989**, *111*, 4353. (f) Kikuchi, K.; Takahashi, Y.; Hoshi, M.; Niwa, T.; Katagiri, T.; Miyashi, T. *J. Phys. Chem.* **1991**, *95*, 2378. (g) Penfield, K. W.; Miller, J. R.; Paddon-Row, M. N.; Cotsaris, E.; Oliver, A. M.; Hush, N. S. *J. Am. Chem. Soc.* **1987**, *109*, 5061. (h) Killing, O. W. *J. Phys. Chem.* **1991**, *95*, 192. (i) Wasielewski, M. R.; Niemczyk, M. P.; Svec, W. A.; Pewitt, E. B. *J. Am. Chem. Soc.* **1985**, *107*, 5562. (j) Delaney, J. K.; Mauzerall, D. C.; Lindsey, J. S. *J. Am. Chem. Soc.* **1990**, *112*, 957. (k) Warman, J. M.; Smit, K. J.; de Haas, M. P.; Jonker, S. A.; Paddon-Row, M. N.; Oliver, A. M.; Kroon, J.; Oevering, H.; Verhoeven, J. W. *J. Phys. Chem.* **1991**, *95*, 1979. (l) Kanda, Y.; Sato, H.; Okada, T.; Mataga, N. *Chem. Phys. Lett.* **1986**, *129*, 306. (m) Kolling, O. W. *J. Phys. Chem.* **1991**, *95*, 192. (n) Schanze, K. S.; Cabana, L. A. *J. Phys. Chem.* **1990**, *94*, 2740.

(15) For example: (a) Miller, J. R.; Beitz, J. V.; Huddleston, R. K. *J. Am. Chem. Soc.* **1984**, *106*, 5057. (b) Beitz, J. V.; Miller, J. R. *J. Chem. Phys.* **1979**, *71*, 4579. (c) Wasielewski, M. R.; Gaines, G. L., III; O'Neil, M. P.; Svec, W. A.; Niemczyk, M. P. *J. Am. Chem. Soc.* **1990**, *112*, 4559. (d) Kakitani, T.; Mataga, N. *J. Phys. Chem.* **1988**, *92*, 5059. (e) McManus, H. J. D.; Kang, Y. S.; Kevan, L. *J. Phys. Chem.* **1992**, *96*, 2274.

(16) For example: (a) Rabani, J. Polyelectrolytes. In *Photoinduced Electron Transfer*; Fox, M. A., Chanon, M., Eds.; Elsevier: Amsterdam, 1988; Vol. B, pp 642–696. (b) Milosavljevic, B. H.; Thomas, J. K. *J. Phys. Chem.* **1985**, *89*, 1830. (c) Tsuchida, A.; Nakano, M.; Yoshida, M.; Yamamoto, M.; Wada, Y. *Polym. Bull.* **1988**, *20*, 297.

(17) For example: (a) Baral, S.; Fendler, J. H. Photoinduced Electron Transfer in Membrane Mimetic Systems. In *Photoinduced Electron Transfer*; Fox, M. A., Chanon, M., Eds.; 1988; Vol. B, p 547.

(18) For example: (a) Baral, S.; Fendler, J. H. Photoinduced Electron Transfer in Membrane Mimetic Systems. In *Photoinduced Electron Transfer*; Fox, M. A., Chanon, M., Eds.; Elsevier: Amsterdam, 1988; Vol. B, pp 545, 560. (b) Seta, P.; Bienvenue, E.; Moore, A. L.; Mathis, P.; Bensasson, R. V.; Liddell, P.; Pessiki, P. J.; Joy, A.; Moore, T. A.; Gust, D. *Nature* **1985**, *316*, 653.

(19) For example: Nespurek, S. *Mater. Sci.* **1984**, *10*, 189.

(20) (a) Lockhart, D. J.; Hammes, S. L.; Franzen, S.; Boxer, S. G. *J. Phys. Chem.* **1991**, *95*, 2217. (b) Popovic, Z. D.; Kovacs, G. J.; Vincett, P. S.; Alegria, G.; Dutton, P. L. *Chem. Phys.* **1986**, *110*, 227.

(21) Nakamura, H.; Uehata, A.; Motonaga, A.; Ogata, T.; Matsuo, T. *Chem. Lett.* **1987**, 543.

(22) (a) Barraud, A.; Palacin, S., Eds. *Langmuir Blodgett Films 5: Proceedings of 5th International Conference on Langmuir-Blodgett Films*; Elsevier: Amsterdam, 1991. (b) Roberts, G., Ed. *Langmuir-Blodgett Films*: Plenum: New York, 1990. (c) Adams, N. K. *The Physics and Chemistry of Surfaces*; Dover: New York, 1968. (d) Adamson, A. W. *Physical Chemistry of Surfaces*; John Wiley & Sons: New York, 1982.

(23) Kuhn, H. *J. Photochem.* **1979**, *10*, 111.

(24) (a) Penner, T. L.; Möbius, D. *J. Am. Chem. Soc.* **1982**, *104*, 7407. (b) Möbius, D. *Ber. Bunsen. Ges. Phys. Chem.* **1978**, *82*, 848.

(25) (a) Saito, M.; Sugi, M.; Iizima, S. *Jpn. J. Appl. Phys.* **1985**, *24*, 379. (b) Sakai, K.; Saito, M.; Sugi, M.; Iizima, S. *Jpn. J. Appl. Phys.* **1985**, *24*, 865. (c) Sugi, M.; Nembach, K.; Möbius, D. *Thin Solid Films* **1975**, *27*, 205.

(26) (a) Janzen, A. F.; Bolton, J. R.; Stillman, M. J. *J. Am. Chem. Soc.* **1979**, *101*, 6337. (b) Janzen, A. F.; Bolton, J. R. *J. Am. Chem. Soc.* **1979**, *101*, 6342.

(27) (a) Fujihira, M.; Sakomura, M.; Kamei, T. *Thin Solid Films* **1989**, *180*, 43. (b) Fujihira, M.; Nishiyama, K.; Aoki, K. *Thin Solid Films* **1988**, *160*, 317. (c) Nishikata, Y.; Morikawa, A.; Kakimoto, M.; Imai, Y.; Nishiyama, K.; Fujihira, M. *Polym. J.* **1990**, *22*, 593. (d) Nishikata, Y.; Fukui, S.; Kakimoto, M.; Imai, Y.; Nishiyama, K.; Fujihira, M. *Thin Solid Films* **1992**, *210/211*, 296.

(28) For example: (a) Miyashita, T.; Yatsue, T.; Matsuda, M. *J. Phys. Chem.* **1991**, *95*, 2448. (b) Van der Auweraer, M.; Verschuere, B.; Biesmans, G.; De Schryver, F. C. *Langmuir* **1987**, *3*, 992. (c) Eichberger, R.; Willig, F.; Storck, W. *Mol. Cryst. Liq. Cryst.* **1989**, *175*, 19. (d) Isoda, S.; Nishikawa, S.; Ueyama, S.; Hanazato, Y.; Kawakubo, H.; Maeda, M. *Thin Solid Films* **1992**, *210/211*, 290. (e) Caminati, G.; Ahuja, R. C.; Möbius, D. *Thin Solid Films* **1992**, *210/211*, 335. (f) Tran-Thi, T. H.; Lipskier, J. F.; Simoes, M.; Palacin, S. *Thin Solid Films* **1992**, *210/211*, 150.

(29) Naito, K.; Egusa, S. *Mol. Cryst. Liq. Cryst.* **1989**, *167*, 51.

(30) Naito, K.; Iwakiri, T.; Miura, A.; Azuma, M. *Langmuir* **1990**, *6*, 1309.

(31) Naito, K.; Miura, A.; Azuma, M. *Langmuir* **1991**, *7*, 627.

(32) Naito, K.; Miura, A.; Azuma, M. *J. Am. Chem. Soc.* **1991**, *113*, 6387.

(33) Naito, K. *J. Colloid Interface Sci.* **1989**, *131*, 218.

(34) Naito, K.; Miura, A.; Azuma, M. *Thin Solid Films* **1992**, *210/211*, 527.

(35) Naito, K.; Miura, A.; Azuma, M. *Thin Solid Films* **1992**, *210/211*, 268.

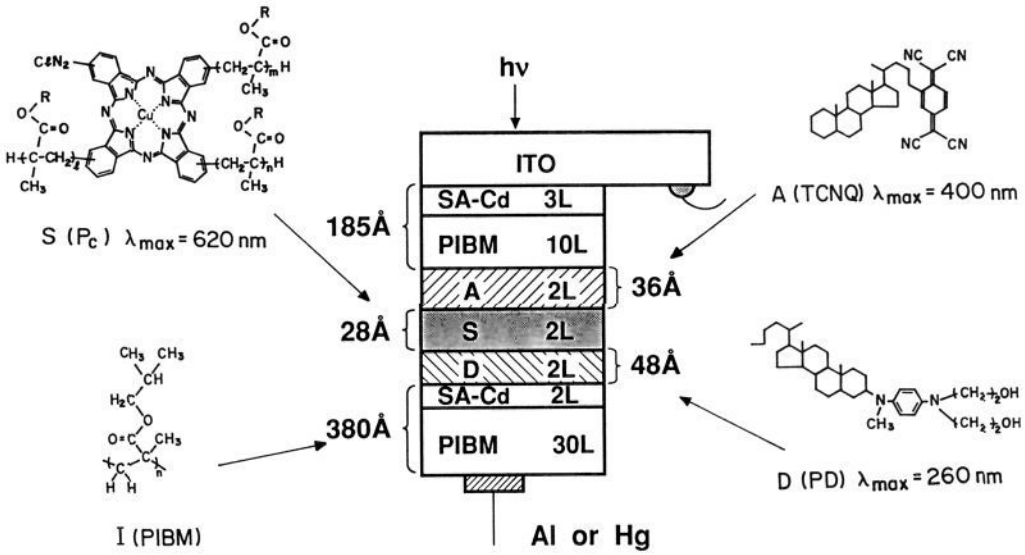

Figure 1. Molecular structures and ASD hetero-LB film device structure.

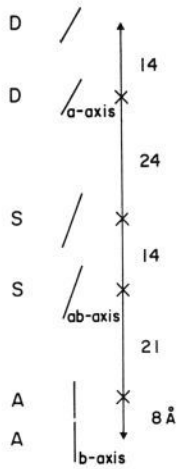

Figure 2. Molecular orientations in ASD device. a axis: long axis in dye plane. b axis: short axis. c axis: normal to dye plane. Molecular orientations in film planes are random.

mm/min for S; deposition surface pressure, 12.5 dyn/cm for A, S, and PIBM and 25 dyn/cm for D and stearic acid. The molecular structures and the ASD hetero-LB film structure are shown in Figure 1. The ASD and AS films were formed on a substrate, and the AI_nS films (n = 0, 1, 2, 3), where I meant a PIBM bilayer (22 Å), were constructed on another substrate. The distances between the dye moieties and the molecular orientations shown in Figure 2 were estimated from the monolayer thickness data by X-ray diffraction and from the polarized IR and UV–visible absorption spectra using homo-LB films, as described elsewhere.[31,33,34]

Electrical Measurement. Apparatus. A mercury drop (diameter 1.5-2 mm) and an evaporated aluminum electrode (diameter 2.5 mm) were used as the counter electrode of the hetero-LB devices. The Al electrode was for measurements at a reduced pressure or in low temperatures. No short circuit was observed for the device using the Al electrode when the PIBM film thickness was equal to or thicker than 330 Å (30 layers). The LB devices were irradiated with red-light pulses from a monochromated halogen lamp (Kenko Techno Light KHL-100R), where an electric shutter (Sigma 65L) and appropriate optical filters were used. He–Ne laser pulses (Neo Ark HN-550R, 633 nm, 6 mW) were also used. Transient photocurrents were magnified with a current amplifier (Keithley 427), and their time dependencies were recorded with a digital storage oscilloscope (Reader Model 300). Photovoltages were measured with a electrometer (Advantest TR8411, input impedance $\geq 10^{15}$ Ω, 10-90% rise time, 0.6 s), and their time dependencies were recorded with an analog recorder. The measurements were usually carried out in a shielded box in an atmospheric condition (20-23 °C, humidity 50-60%). A cryostat

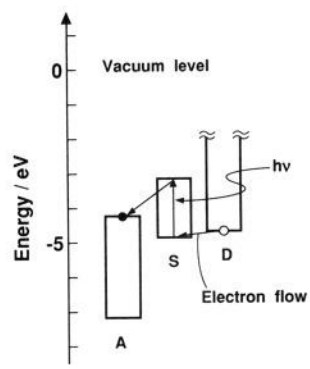

Figure 3. Energy levels of conduction and valence bands for A, S, and D dye crystals as reported in the literature,[36] and an expected PET flow.

equipped with a thermoelectric thermometer was utilized under a reduced pressure (≈10^{-3} Torr) at various temperatures. Each observation of the voltage decay was carried out after heating the devices at room temperature to make the separated charges recombine completely. The voltage decay curves at room temperature varied little during the heat cycles repeated.

Electric Field Dependence. CR processes under an applied electric field were investigated by measuring transient photocurrent recoveries. The initial peak photocurrent without any charging states is described by I_0. The reduced peak photocurrent (I_t) was observed under the condition where the separated charges remain in the film. Therefore, we were able to estimate the CR rate by measuring I_t/I_0.

The measurement of I_t/I_0 was carried out as follows. The separated charges were discharged by applying a negative bias of –0.8 V to the ITO electrode of the hetero-LB devices for 1 min. A desired bias was then applied, and a pulsed light of 610 nm ($^1/_8$ s, 6 mW/cm^2) was emitted to measure I_0. After t s, a second light pulse was then emitted to measure I_t. This procedure was repeated several times. The I_0 value was almost constant for the repeated cycles and unchanged with the waiting time (10-2000 s) in the dark at +1 V to the ITO electrode, indicating no space–charge effect.

Results

Photoinduced Electron Transfer (PET). Transient Photocurrent. A transient current was induced in an ASD device by irradiating the sample with red light, which was selectively absorbed by S. The current flow from D to A, resulting in an A^-SD^+ state, was expected from the energy levels shown in Figure 3. The energy levels of valence and conduction bands were obtained from the ionization potentials (I_p) and electron affinities (E_A) reported for crystals of ASD dye moieties.[36]

A significantly smaller reverse current was also observed when

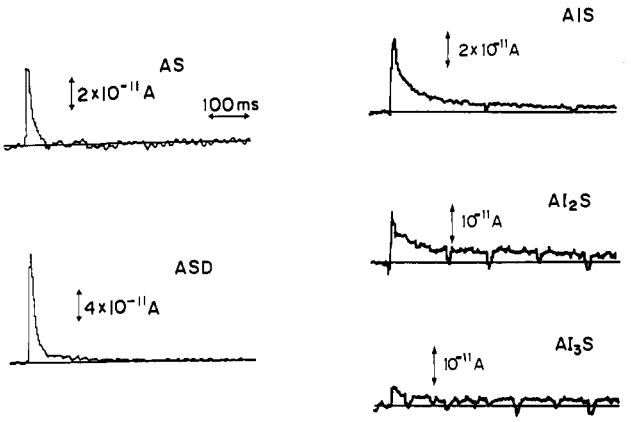

Figure 4. Dependence of transient photocurrent on hetero film structures at room temperature. Condition: 0-V bias; Hg electrode; He-Ne laser, 6 mW/cm², 2-s pulse; rise time of current amplifier, 10 ms.

the light was turned off. SD and S devices in the absence of A showed a much smaller peak current (<1%).

The action spectrum, indicating the photoresponses of the ASD device, was attributed to the photoexitation of S. The peak current increased with increasing light intensity, while its photoelectric efficiency decreased. This efficiency decrease indicates that the photocurrent is not intrinsic for S. The peak current decreased as the applied voltage increased (ITO negative). No current was observed at −2 V. In the dark, the film was a good insulator (resistivity > 10^{15} Ω cm at 1 V), and no rectifying property was observed. Although the peak current of the ASD device at 113 K was larger than that at 293 K, the photocurrent feature did not change very much.

Relations between PET and Hetero Film Structures. Figure 4 shows the transient photocurrent responses of various hetero structures. The response for the ASD device within 30 ms was almost the same as that for the AS device, while it took 200-300 ms for the photocurrent of the ASD device to reach the zero line. Insertion of a PIBM bilayer (I) (22 Å) between A and S (AIS) caused the photocurrent decay to be slow and the peak current to be small. This tendency became more intensive when the layer number of I increased (AI_2S, AI_3S). The photocurrent rise-up proceeded within a short period, faster than the observed time resolution of the apparatus (the time for opening the shutter).

Charge Recombination (CR). Photovoltage Decay. In the ASD device including strong donor and acceptor molecules separated from the electrode by the insulator layers, the photodissociated electrons and holes are expected to be stored in separated positions in the dark. The lifetime of such separated charges was measured by photovoltage decay [$V(t)$]. The voltage increased rapidly at first and then gradually with continuous photoirradiation. The voltage began to decrease without delay when the light was turned off. Figure 5 indicates the photovoltage decay curves for the ASD and AS devices at various temperatures. The decay rate for the ASD device was much smaller than that for the AS device at room temperature. The initial $V(t = 0)$ values increased at low temperatures, and the voltage decay slowed down. The separated charges can be considered to recombine almost completely even at low temperatures, because 90% of $V(t = 0)$ was observed at the next photoirradiation after 30 min at 160 K for the ASD device.

Deviation from a Single Exponential Decay Curve. The CR process in dilute solutions is known to be expressed by the following first-order kinetics:[14]

$$dP/dt = k_{CR}(1 - P) \quad (1)$$

where $P = [V(t = 0) - V(t)]/V(t = 0)$ and k_{CR} denote the CR

(36) (a) Seki, K. *Mol. Cryst. Liq. Cryst.* **1989**, *171*, 255. (b) Pope, M.; Swenberg, C. E. *Electronic Processes in Organic Crystals*: Clarendon: Oxford, 1982; pp 452, 559.

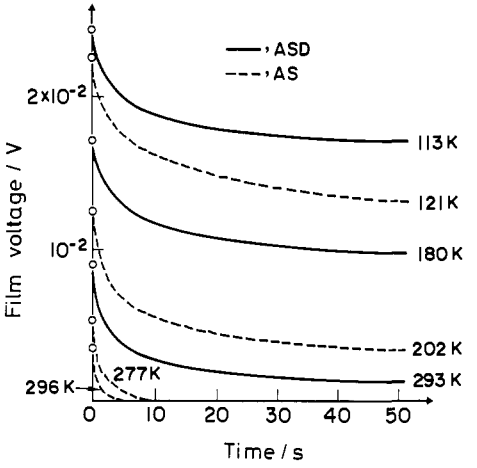

Figure 5. Photovoltage decays of ASD and AS devices at various temperatures. Condition: 0-V bias; Al electrode; 610 nm, 3 mW/cm², 2-s pulse.

probability of the separated charges (extent of CR) and the rate constant, respectively. When time (t) is 0, P is 0; therefore,

$$-\ln(1 - P) = k_{CR}t \quad (2)$$

However, the plots of $-\ln(1 - P)$ vs t for the present hetero-LB devices were not linear. For such cases, analyses taking account of the distributions of energy and/or distance are required rather than simplified curve fitting with two or three exponential components. However, uncriticized usage of a certain distribution function such as Gaussian and rectangular distributions sometimes leads to unlikely descriptions of the results. For analyzing nonlinear reaction kinetics, the relaxation effect of molecular orientation should be considered occasionally.[15a]

This paper gives the results of examining which item was predominant among energy distribution, distance distribution, and relaxation by changing the temperature and hetero structures. The distribution features were also obtained experimentally when possible when they were dominant.

Temperature Dependence. A. Apparent Change of Rate Constant k_{CR}. According to predecessor studies, k_{CR} can be divided, as shown in eq 3,[37]

$$k_{CR} = k_0 \exp(-\alpha r) \exp(-E_a/k_B T) \quad (3)$$

where k_0 is a constant and usually $\approx 10^{13}$ s^{-1},[38] and its temperature dependence is not considered here. α is a constant and usually 0.5-2 Å^{-1},[39] r means the edge-to-edge distance between chromophores, E_a means the activation energy, k_B is the Boltzmann constant, and T means the absolute temperature. According to eqs 1 and 3,

$$\ln[(1/(1-P))dP/dt] = \ln k_{CR} = \ln(k_0) - \alpha r - E_a/k_B T \quad (4)$$

If there are some distributions of r and/or E_a, the apparent rate constant k_{CR} decreases with an increase in P, because separated electron-hole pairs with smaller r and smaller E_a combine with each other more rapidly. The variables r and E_a for the devices can be expressed as functions of P.

If the distribution of r is dominant and that of E_a is not, then the plot of $\ln k_{CR}$ vs P does not change its feature very much with varying temperature except for some shift. However, the

(37) Wasielewski, M. R. Distance Dependencies of Electron Transfer Reaction. In *Photoinduced Electron Transfer*; Fox, M. A., Chanon, M., Eds.; Elsevier: Amsterdam, 1988; Vol. A, p 162.

(38) Wasielewski, M. R. Distance Dependencies of Electron Transfer Reaction. In *Photoinduced Electron Transfer*; Fox, M. A., Chanon, M., Eds.; Elsevier: Amsterdam, 1988; Vol. A, p 165.

(39) Wasielewski, M. R. Distance Dependencies of Electron Transfer Reaction. In *Photoinduced Electron Transfer*; Fox, M. A., Chanon, M., Eds.; Elsevier: Amsterdam, 1988; Vol. A, pp 161–206.

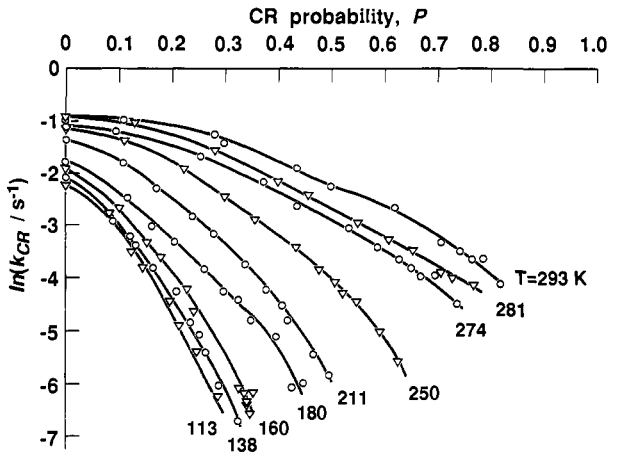

Figure 6. Dependence of apparent rate constant k_{CR} on CR probability (P) for ASD device at various temperatures. Condition: 0-V bias; Al electrode; 610 nm, 3 mW/cm², 2-s pulse. The lines are merely to guide the smooth curves through the data points.

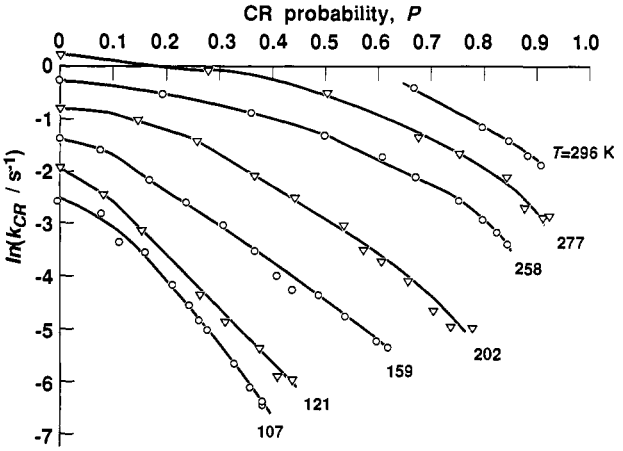

Figure 7. Dependence of apparent rate constant k_{CR} on CR probability (P) for AS device at various temperatures. Condition: 0-V bias; Al electrode; 610 nm, 3 mW/cm², 2-s pulse. The lines are merely to guide the smooth curves through the data points.

experimental results shown in Figures 6 and 7 indicated that the assumption was correct neither for the ASD device nor for the AS one. The distributions of E_a were considered dominant for these devices. dP/dt values were obtained from the slopes of the tangents to the decay curves in Figure 5.

The reproducibility of the plot for the ASD device at room temperature was obtained for various V_0 values (1.5-15 mV) obtained by changing the light pulse width and for four different samples. The features of the plot did not change very much except for some shift.

In place of the distribution of E_a, there is a probability that E_a increases with time, i.e., energy relaxation. The E_a change at 293 K for 45 s was faster by only 1.7 times that at 113 K. It is known that the relaxation speed is very sensitive to temperature. Therefore, the relaxation process is considered not to be dominant in this case.

B. Change in Activation Energy. Figures 8 and 9 show Arrhenius plots for each P value obtained from Figures 6 and 7. Each plot became linear and crossed at T_0 (= 350 K) both for the ASD device and for the AS one. This indicates that the distributions of E_a disappear at T_0 and that k_{CR} becomes a constant, k_{350}, at T_0. The following equation has been established:

$$\ln k_{CR} = \ln(k_{350}) - E_0(P)[(1-T/T_0)/k_B T] \qquad (5)$$

where $E_0(P)$ was obtained from the slopes of the Arrhenius plots. E_a is a function of P and T and is expressed by

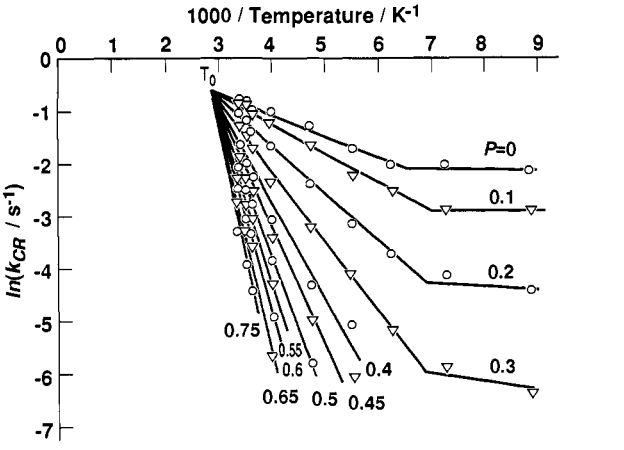

Figure 8. Arrhenius plots of apparent rate constant k_{CR} at various CR probabilities (P) for ASD device, obtained from Figure 6.

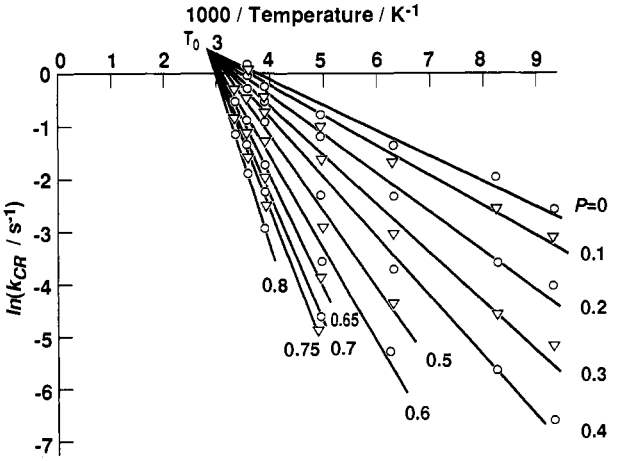

Figure 9. Arrhenius plots of apparent rate constant k_{CR} at various CR probabilities (P) for AS device, obtained from Figure 7.

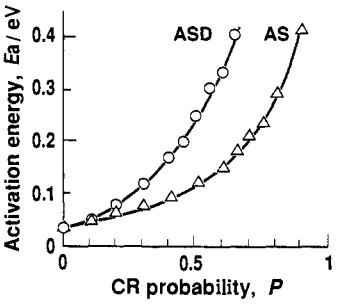

Figure 10. Dependence of activation energy (E_0) at $T \rightarrow 0$ K on survival probability (P) for ASD and AS devices, obtained from Figures 8 and 9. The lines are merely to guide the smooth curves through the data points.

$$E_a(P,T) = E_0(P)(1-T/T_0) \qquad (6)$$

$E_0(P)$ corresponds to the extrapolation of $T = 0$ K and is shown in Figure 10. At higher temperatures, the E_a values and their distribution width became smaller. If the temperature dependence of k_0 obeys the Marcus theory,[40] then k_0 is proportional to $T^{-1/2}$. The E_0 values should increase only by about 10 meV.

As for the ASD device, there was a clear tendency for CR to become a nonactivation process at low temperatures (<150 K).

C. Activation Energy Distribution. The separated electrons and holes with smaller E_a combine with each other more rapidly than those with larger E_a. A step CR process was assumed: at

(40) (a) Marcus, R. A. *J. Chem. Phys.* **1956**, *24*, 966. (b) Marcus, R. A. *Annu. Rev. Phys. Chem.* **1964**, *15*, 155.

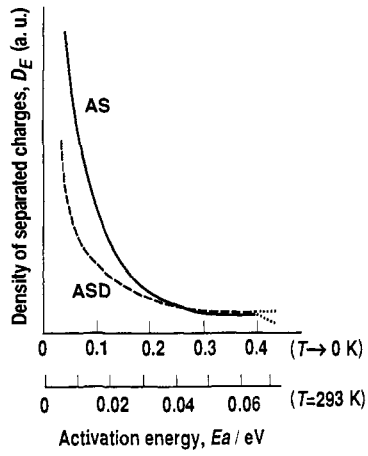

Figure 11. Distributions of activation energy (E_a) for ASD and AS devices.

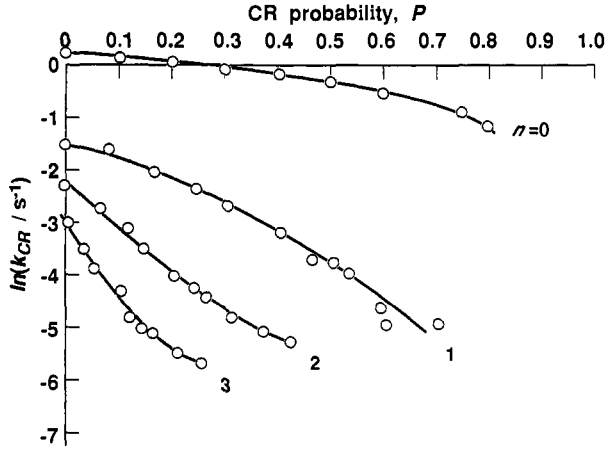

Figure 12. Dependence of apparent rate constant k_{CR} on CR probability (P) for AI_nS devices at room temperature. I means PIBM bilayer. Condition: 0-V bias; Hg electrode; 610 nm, 6 mW/cm^2, 2-s pulse. The lines are merely to guide the smooth curves through the data points.

T and at P, the separated charges with $E_a < E_a(P,T)$ disappeared completely, and those with $E_a \geq E_a(P,T)$ remained completely. The existence probability of the separated charges between E_a and $E_a + dE_a$ was defined by $D_E(E_a)dE_a$, which was obtained by

$$D_E(E_a) = dP/dE_a \quad (7)$$

Figure 11 shows the distribution functions D_E calculated from Figure 10 and eq 7. The minimum E_a value for the ASD device was similar to that for the AS device. For both devices, D_E decreased as E_a increased. D_E for the ASD device decreased more abruptly in the smallest E_a region than that for the AS device but more gradually in the largest E_a region. The D_E features with $E_a > 0.4$ eV at $T \rightarrow 0$ K could not be determined because of the slow CR rates and/or the base line variations of the voltage measurement. Such nondetermined D_E portions for the ASD and AS devices correspond to 35% and 10%, respectively. The width of E_a became narrower with temperature rise.

Interdistance Dependence between Chromophores. A. Apaprent Change of Rate Constant k_{CR}. Figure 12 shows the plots of ln k_{CR} vs P for AI_nS devices, where I means a PIBM bilayer film (22 Å) and n means the number of I. The apparent rate constant k_{CR} decreased as n increased. The features of the plots were different from each other.

B. Interdistance Distribution between Chromophores. The distributions of E_a for the AI_nS devices were assumed to be the same as that for the AS device. It was also assumed that there was no distance distribution between A and S for the AS device. The distance distributions for the AI_nS devices were obtained under the assumptions. The difference in the ln k_{CR} value at P

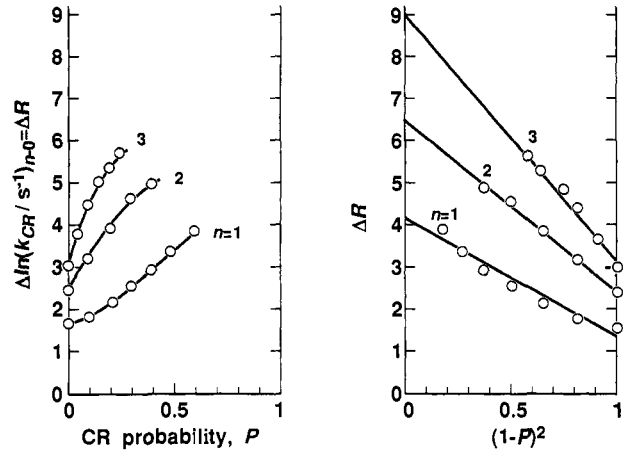

Figure 13. Dependence of k_{CR} difference between AI_nS devices and the AS device on CR probability (P), obtained from Figure 12. The lines in the left plot are merely to guide the smooth curves through the data points.

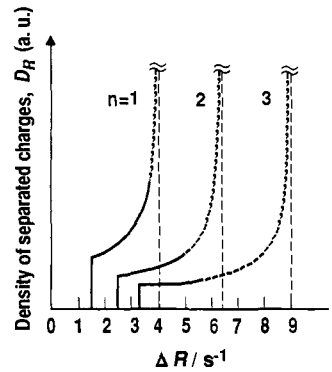

Figure 14. Interdistance distributions between A and S for AI_nS devices.

between the AI_nS and AS devices corresponds to the αr difference ($\Delta R(P)$) according to eq 4 and is shown in Figure 13. According to Figure 13,

$$\Delta R(P) = \Delta R_{max} - \beta(1 - P)^2 \quad (8)$$

was established, where (ΔR_{max}, β) for n = 1, 2, and 3 were (4.1, 2.6), (6.4, 3.9), and (9.0, 5.7), respectively, all in units of s^{-1}. The distance distribution functions D_R were obtained through a similar method as for the activation energy distribution and are shown in Figure 14. In the figure, the solid lines correspond to the observed k_{CR} values and the broken lines to the values expected from eq 8. The distribution width becomes wider as n increases, and D_R increases abruptly near ΔR_{max}.

C. Distance Constant α. In Figure 14, the ΔR_{max} values are probably influenced by the correct thickness of the insulator layers (I = 22 Å). The ΔR_{max} vs n plot gave a linear line, and α = 0.15 Å^{-1} was obtained from its slope. This value was much smaller than the usual values (0.5-2 Å^{-1}).

Electrical Field Dependence. The lifetime was also estimated from the photocurrent peak recovery as shown in Figure 15. The recovery of the AS device was extremely faster than that of the ASD one at room temperature. This result was in accordance with the photovoltage decay curves shown in Figure 5. The recovery took much time under positive ITO biases, which were profitable for stabilizing the charge-separated state, while it speeded up under negative biases.

Discussion

Charge Recombination (CR). Activation Energy Distribution. The polarization energies in solid phases cause I_p and E_A to be smaller and larger, respectively, than those in gas phases. In the

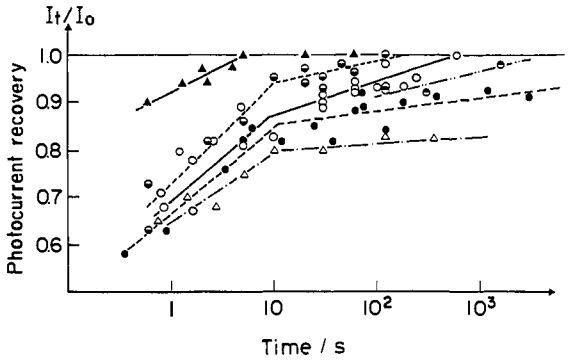

Figure 15. Bias voltage dependence of photocurrent recovery at room temperature. Condition: Hg electrode; 610 nm, 6 mW/cm², 1/8-s pulse; rise time of current amplifier, 30 ms. ITO voltage for ASD device: ⊖, −0.5 V; ○, 0 V; ⊖, 0.5 V; ●, 1 V; △, 2 V. ▲ for AS device at 0 V.

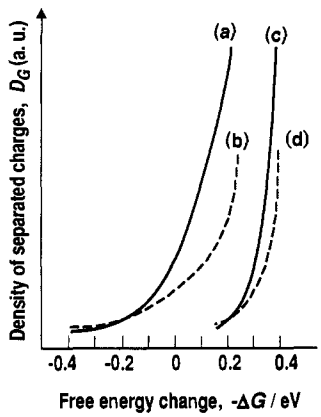

Figure 16. Free energy change distribution of CR process for ASD and AS devices, according to the Marcus theory and Figure 11, assuming that reorganization energy λ is 0.5 eV. (a) AS at $T \rightarrow 0$ K, (b) ASD at $T \rightarrow 0$ K, (c) AS at 293 K, (d) ASD at 293 K.

present LB films, the in-plane orientations of the dye skeletons were found to be random. Therefore, various aggregation states can be considered to form wide distributions of the polarization energy.[41] This will be a cause of the activation energy distributions shown in Figure 11.

According to the classical Marcus theory,[40] the activation energy of electron transfer can be described by

$$E_a = (\Delta G+\lambda)^2/4\lambda \qquad (9)$$

where $-\Delta G$ means the free energy change of electron transfer and λ means the reorganization energy of the surrounding medium. The λ value is between 1.5 and 2 eV in polar solvents,[12,14] while it is between 0.2 and 1 eV in solid phases.[12,15] According to the theory, E_a decreases as $-\Delta G$ increases, reaches 0 at $-\Delta G = \lambda$, and then increases. Therefore, the $-\Delta G < \lambda$ region is called "the noraml region", and $-\Delta G > \lambda$ is called "the inverted region". The existence of the inverted region has been controversial,[42] while the normal region has been in accordance with experimental results.[43] The CR process of the hetero-LB films can be considered in the normal region due to their strong donor and acceptor moieties. λ was assumed to be 0.5 eV, and the distribution of $-\Delta G$ was obtained from Figure 11 and eq 9. Figure 16 shows the $-\Delta G$ distributions at 293 K and at $T \rightarrow 0$ K.

The free energy levels of various states were obtained according to Figure 3, as shown in Figure 17. In the figure, the Coulomb stabilization energy (0.11 eV for the A^-S^+, 0.06 eV for the A^-SD^+)

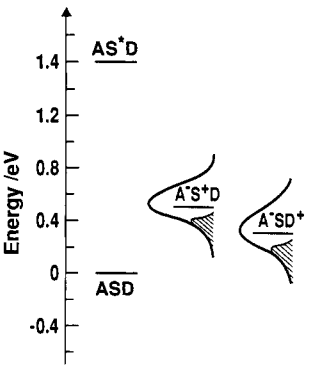

Figure 17. Schematic levels of free energies for various states at room temperature. The bold curves mean the energy level distribution (Gaussian) of the separated-charge states. The separated charges may exist in the shadow region denoting the product of the Gaussian and Fermi distribution functions.

was taken into account, assuming that the relative dielectric constant was 4. If the distribution of the polarization energies is Gaussian, then the energy levels of the separated-charge states are also distributed as Gaussian types. The separated charges were much fewer than the molecules under the experimental conditions. In-plane repulsion of the charges was negligible.[10] Therefore, the separated charges can be considered to be distributed, obeying the product of Gaussian and Fermi distribution functions, as shown in the shadow regions in Figure 17.[44]

The distributions in Figure 17 were nearly in accordance with the $-\Delta G$ distribution (D_G) shown in Figure 16. The few separated charges with the largest $-\Delta G$ values disappeared very rapidly beyond the observation limit. For that reason, the observed D_G functions can be considered to be approximately exponential curves.[45]

In Figure 16, the maximum $-\Delta G$ value for the ASD device is similar to that for the AS device. $-\Delta G$ for the ASD device decreases more abruptly in the largest $-\Delta G$ region than that for the AS device but gradually in the smallest $-\Delta G$ region. This is due to the coexistence of A^-S^+D and A^-SD^+ states at the beginning of the CR process.

The $-\Delta G$ distributions were wider in low temperatures than those in high temperatures and disappeared at T_0. In low temperatures, rotations of the molecules are fixed and various aggregation states are present. The polarization energies are therefore widely distributed. In high temperatures, the molecules can rotate rather freely and the aggregations are solved. Therefore, the widths of the $-\Delta G$ distributions are narrow and the $-\Delta G$ values are large in high temperatures. The existence of a temperature (T_0') similar to T_0 has been known in amorphous polymer photoconductors like poly(vinylcarbazole).[46] At the temperature T_0', the activation energy lowering of photoconduction by an applied electric field disappears, and T_0' values increase as their glass transition temperatures (T_g) increase.[47] The ASD and AS devices have the same T_0 value (350 K). This is probably due to the fact that T_g values of A and of the insulator PIBM are about 310 and 326 K, respectively.

In dilute solutions, single exponential decays have been observed at room temperature, indicating no E_a distribution. However, in higher concentrated solutions[14b] and/or in frozen solutions,[15] deviations from single exponential decays take place.

The energy levels shown in Figure 17 should be shifted by applying an electric field. Applying 1 V to the ASD device with

(41) Pope, M.; Swenberg, C. E. *Electronic Processes in Organic Crystals*; Clarendon: Oxford, 1982; p 246.
(42) (a) Kakitani, T.; Mataga, N. *J. Phys. Chem.* **1986**, *90*, 993. (b) Kakitani, T.; Mataga, N. *J. Phys. Chem.* **1987**, *91*, 6277.
(43) (a) Rehm, D.; Weller, A. *Isr. J. Chem.* 1970, *8*, 259. (b) Eberson, L. *Acta Chem. Phys.* **1982**, *B36*, 533.
(44) Pope, M.; Swenberg, C. E. *Electronic Processes in Organic Crystals*; Clarendon: Oxford, 1982; p 246.
(45) Pope, M.; Swenberg, C. E. *Electronic Processes in Organic Crystals*; Clarendon: Oxford, 1982; p 241.
(46) (a) Gill, W. D. *J. Appl. Phys.* **1972**, *43*, 5033. (b) Bässler, H.; Schönherr, G.; Abkowitz, M.; Pai, D. M. *Phys. Rev. B* **1982**, *26*, 3105.
(47) Fujino, M.; Kanazawa, Y.; Mikawa, H.; Kusabayashi, S.; Yokoyama, M. *Solid State Commun.* **1984**, *49*, 575.

a 700-Å thickness causes the levels to shift by 0.1 eV. The result shown in Figure 15 is in accordance with this.

As for the ASD device, the tendency was found that the charge recombination became activationless at low temperatures. A similar phenomenon has been observed in natural photosynthetic reaction centers and has been explained by the coexistence of different reaction mechanisms.[12] For the present LB films, further investigation at low temperatures is necessary.[48]

Interdistance Distribution between Chromophores. The D_R distributions for the AI_nS devices shown in Figure 14 indicate the existence of some defects in the I layers. The unusually small value of the distance constant α (0.15 $Å^{-1}$) also suggests that electron transfers take place through the S molecules in the I layers. According to the usual electron-transfer theories, electron transfers in the AI_nS devices cannot take place due to the too-far distance between the chromophores if the I layers have no defect. In the cases of using LB films as an insulator, very small α values have sometimes been reported,[25a] probably due to some defects in the LB films. The PIBM LB films used as I in the present study are more homogeneous than fatty acid LB films but are not perfect.[49]

The CR rate for the ASD device was faster than that expected from the distance between A and D compared with the AS device. This is probably due to electron transfer through S, which is known as a "super exchange mechanism".[50]

Photoinduced Electron Transfer (PET). The photocurrent in hetero-LB films was able to be observed when the PET rate was larger than the CR rate. The PET rate cannot be obtained simply by observing the transient photocurrent. Further study is necessary to determine it.

According to the classical Marcus theory, PETs in the present hetero-LB devices exist in the inverted region, where large E_a values should be observed. However, no feature change was observed in the transient photocurrent response at different temperatures. It has been known that the inverted region is not observed in charge separation reactions, and many theories have been proposed to explain it.[11] As for the present PET in the LB films, it can be considered that the inverted region does not exist, either.

No photocurrent was observed by applying −2 V to the ITO electrode for the ASD device at room temperature. The applied voltage will cause the energy level of the A^-S^+D state to rise up by about 0.2 eV (see Figure 17) and will cause the CR rate to be as large as the PET rate.

PET occurred for the ASD device, but hardly at all for the SD device. This means that electron transfer takes place from D to S^+ but not from D to the photoexcited S*. For the SD device, the large Coulomb energy between an electron and a hole in S* will cause the hole level of S to rise.

The PET and CR processes for many porphyrin derivatives substituted by donor and acceptor moieties in solutions have been investigated in detail by Gust and Moore, et al.[14a,b] and by Wasielewski et al.[14i,15c] The lifetimes of the separated charges for the derivatives are extremely longer than those for other solution systems while much shorter than those for the present LB films. Their electron-transfer mechanism, however, is similar to that in the LB films. The first electron transfer occurs from photoexcited S* to A, and the second transfer from D to S^+.

Conclusion

We have reported herein that the photoinduced electron transfers and the recombination reactions of separated electrons and holes can be controlled by hetero film structures, by temperatures, and by electric fields. The behavior was able to be quantitatively understood in the framework of the electron-transfer theories by considering the energy and distance distributions. The present approach to characterize the electron-transfer processes has been considered to be applicable both to the natural systems and to any artificial molecular systems with layered structures.

Acknowledgment. We thank Mr. Makoto Azuma, Dr. Syun Egusa, Mr. Toshio Nakayama, Ms. Yoko Watanabe, Mr. Kazushige Yamamoto, and Mr. Takasi Sasaki (Toshiba R & D Center) for their helpful discussions on this study. Thanks are also due to Dr. Norio Tanaka (Dainichi Seika) for supplying S. We are also indebted to Mr. Fujio Umibe (consultant) for reviewing the original manuscript and suggesting revisions in its English.

(48) Naito, K.; Miura, A. *Thin Solid Films*, submitted for publication.
(49) Matsuda, H.; Kawada, H.; Takimoto, K.; Morikawa, Y.; Eguchi, K.; Nakagiri, T. *Thin Solid Films* **1989**, *178*, 505.
(50) (a) Wasielewski, M. R. Distance Dependencies of Electron Transfer Reaction. In *Photoinduced Electron Transfer*; Fox, M. A., Chanon, M., Eds.; Elsevier: Amsterdam, 1988; Vol. A, p 165. (b) Onuchic, J. N.; Beratan, D. N. *J. Am. Chem. Soc.* **1987**, *109*, 6771.